

Thermally Active Liquid Crystal Network Gripper Mimicking the Self-Peeling of Gecko Toe Pads

Hamed Shahsavan, Seyyed Muhammad Salili, Antal Jákli,* and Boxin Zhao*

The climbing ability of geckos is mainly attributed to their adhesive toe pads, which are embroidered with hierarchical hair-like structures. Such surface structures promote compliance, facilitate intimate contact, and maximize omnipresent van der Waals interactions with mating surfaces.^[1,2] It is known that particular configurations of geckos' toes play important roles in regulation of adhesion during their locomotion. Physical appearances of the gecko toes in attachment/gripping and detachment/releasing mode are shown in **Figure 1a,b**. In attachment, two diagonally opposite toes are attached and pull inward toward the animal's body center of the mass, while the other two are detached. In a configuration known as Y-configuration, gecko applies both normal and lateral forces to push and drag the setae array against the mating surfaces.^[2–5] During detachment, setae arrays are arranged in a critical angle to facilitate releasing of toe pads. Toes curl and scroll upward and away from the surface to rapidly reduce the high adhesion/friction using the setal shaft acting as the lever for perpendicular peeling off the spatulae from the substrates.^[6] The back-scrolling motion and self-peeling of the toes at any instant during detachment concentrates the detachment force only on a small portion of all attached setae.^[1] The back-scrolling motion is not only important for releasing, but also for self-cleaning, as contamination can be shed twice as fast when this motion is used.^[7]

Development of gecko-inspired adhesives is now a well-established field of research as a result of numerous reports published in the past two decades.^[8–11] These structures usually are based on simple micro/nanopillars that are terminated by flaps^[12] or thin films,^[13,14] and are bundled in either single or multiple levels.^[15] Despite the great achievements in fabrication of isolated and static fibrillar structures, active control of adhesion by mimicking smart and switchable properties of gecko toe pads still remains a challenge. Toward this end, one

approach is based on gecko-inspired structures with tuneable surface topography upon exposure to external cues, such as heat, light, or magnetic fields.^[16–19] Second approach is based on directionality of dry fibrillar adhesives. Using this approach, shear-induced grip and release and buckling-based release were employed in industrial and manipulation systems,^[20,21] or slanted micropillars were exploited for transfer printing.^[22] The other approach is based on self-peeling and back-scrolling mechanism of gecko toe pads, which is practically used in a limited number of applications such as releasing phase of robotic locomotion mechanism.^[23] Despite the accomplishments in mimicking the anisotropic mechanism of frictional adhesion of gecko toes during the gripping, the muscle-driven detachment mechanism, which is based on back-scrolling of gecko toes, has not been fully exploited and reproduced. This is important as the climbing dynamics and self-cleaning of the gecko toes is crucially dependent on this mechanism.^[24] The resultant releasing capabilities can also have direct implication in other technologies such as pick and place handling of delicate objects and transfer printing.

Crosslinked networks of liquid crystal polymers (LCNs) with different level of cross-linking have been used as bending actuators, accordion-like ribbons, sophisticated voxelated 3D structures,^[25–27] and in applications, such as microfluidics, micro-electro-mechanical systems, adaptive surfaces, and even transportation of 3D objects.^[28–31] Also, remote control and manipulation of adhesion, friction, surface undulations, and wetting of LCN micropillars have been subject of interest in a few reports.^[17,32–34] However, potential application of LCNs for regulation of adhesion by stimuli responsive back-scrolling and self-peeling, resembling the motion of gecko toe pads, has not been addressed well in the literature. In the only report recently published by us, dynamic self-cleaning was demonstrated by temperature-controlled deformations of microtextured LCNs.^[34]

In this study, we report the integration of gecko-inspired adhesives to a hybrid nematic side-chain LCN cantilevers so as to design a multilegged gecko gripper having thermally induced self-peeling capacity. We also fabricate a prototype of the gecko gripper to handle (pick and place) thin delicate objects by determining the optimum mechanical strength of the LCN and the maximum size of the adhesive patch.

The schematics of the developed multilegged gripper and the proposed mechanism of pick-and-place are illustrated in **Figure 1c,d**. Each leg is made by a hybrid aligned (splay deformation) LCN cantilever fixed at one end, and a film-terminated fibrillar adhesive patch attached to the other end. Details of fabrication and the synthesis procedures are shown in **Figure S1** (Supporting Information) given in Section SI-1 (Supporting Information). $188 \pm 4 \mu\text{m}$ thick films of mesogenic material (M1) with various cross-linking contents (M2) were fabricated by capillary filling the LCN precursors in their isotropic phase, followed by

H. Shahsavan, Prof. B. Zhao
Department of Chemical Engineering
Waterloo Institute for Nanotechnology
Institute for Polymer Research, and Centre for
Bioengineering and Biotechnology
200 University Avenue W, Waterloo
ON N2L 3G1, Canada
E-mail: zhaob@uwaterloo.ca

H. Shahsavan, S. M. Salili, Prof. A. Jákli
Chemical Physics Interdisciplinary Program and
Liquid Crystal Institute
Kent State University
Kent, OH 44242, USA
E-mail: ajakli@kent.edu

Prof. A. Jákli
Complex Fluids Group
Wigner Research Centre
H-1121, Budapest, Hungary



DOI: 10.1002/adma.201604021

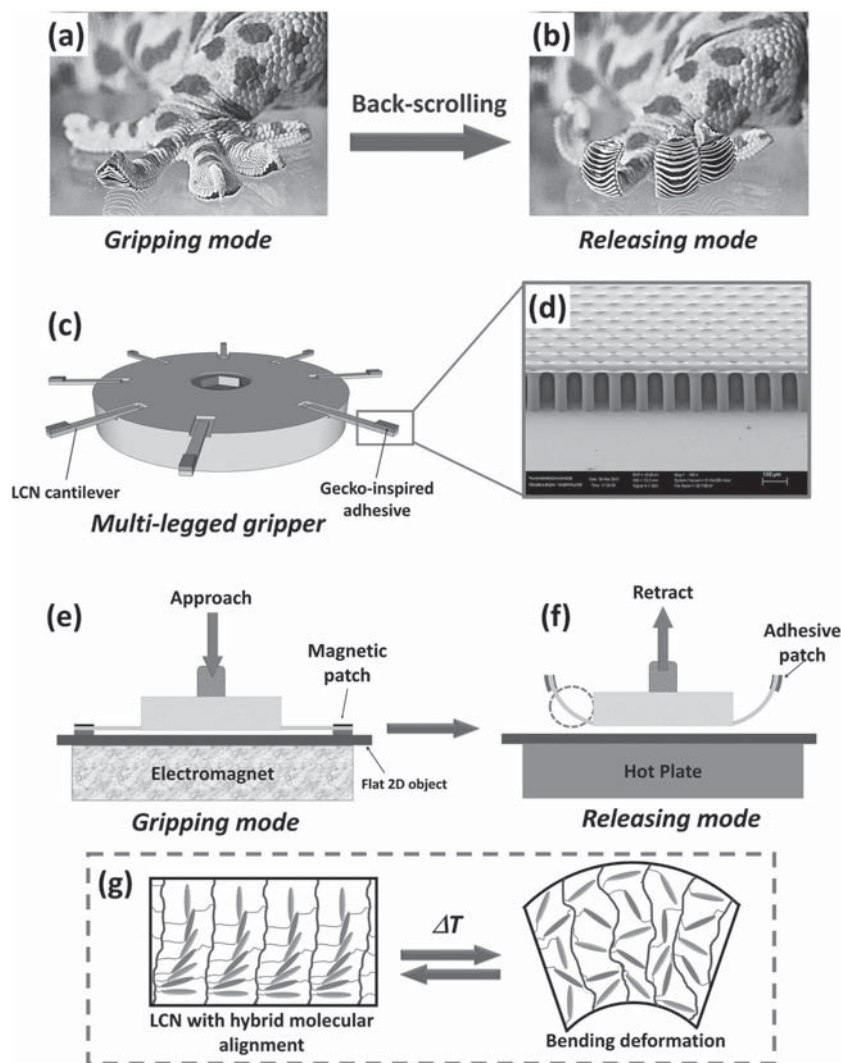


Figure 1. Optical images of gecko toes a) fully extended in gripping and b) back-scrolled in releasing modes; c) schematic view of the designed multilegged LCN-based gripper with d) biomimetic film-terminated fibrillar adhesives; proposed mechanism of e) gripping facilitated by an electromagnet and f) releasing induced by thermal deformation of hybrid LCN cantilevers; g) mechanism of shape change in a nematic hybrid LCN during nematic–isotropic transition, which is along with expansion on the homeotropic side and contraction on the planar side.

photopolymerization reaction at their nematic phase. Two glass substrates with homeotropic and planar surface anchoring properties were used to induce a hybrid alignment needed to achieve bending deformation of the LCN film upon heating. The chemical structure of the monomers and the synthesis scheme are shown in Figure S1a (Supporting Information). Two types of film-terminated fibrillar adhesive structures of PDMS, fully elastic (E-FT), and with a viscoelastic top-coat (VE-FT), were fabricated using soft-lithography and inking techniques.^[14,35] Polydimethylsiloxane (PDMS) micropillars (50 μm diameter, 150 μm height, and 100 μm center-to-center spacing) were fabricated by casting and curing of the PDMS liquid precursor on a Si negative master-mold. The obtained fibrillar PDMS surfaces were placed up-side-down on thin films of liquid PDMS that were spun on low surface energy glass substrates and peeled off

gently after curing (E-FT). Finally, a thin layer of liquid PDMS with lower amount of curing agent was spun onto the film-terminated structure, and whole structure was cured at elevated temperature (VE-FT). Figure 1d shows scanning electron microscope (SEM) image taken from the sample E-FT.

The gripping of lightweight thin and flat objects such as a silicon wafer can be achieved through normal preloading of the adhesive patch to the substrate. Due to the flexibility of the LCN cantilever and lightness of the adhesive assembly, natural downward curvature of the LCN did not provide adequate preload stress during approaching. For this reason, we attached small magnetic patches to the upper side of cantilevers as shown in Figure 1e; in this way, preload stress can be provided via attractive magnetic field created by an electromagnet underneath the sample (Movie S1, Supporting Information). Details on fabrication of the magnetic patch and measurement of the stress produced in the magnetic field are explained in section SI-1 (Supporting Information). Releasing was triggered by temperature-driven bending of the LCN cantilever that caused peeling off the adhesive patch, as can be seen in Figure 1f. The molecular mechanism of thermal actuation of LCN is illustrated in Figure 1g.

There are some basic criteria that should be met to enable the gripping and releasing. For gripping, the magnetic field should be sufficient to impose necessary preload; the adhesive strength of the adhesive patches need to be high enough to bear the gravitational force acting on the lifted object; the LCN cantilevers must be resilient enough to retain their structural integrity when bearing the weight of the lifted objects. For releasing, the LCN cantilever output bending force must be high enough to overcome the adhesion of the patches and the deformation must be large enough to create sufficient momentum to develop crack front during the peeling.

We expect higher load bearing and bending forces but smaller bending amplitude from stiffer LCN cantilevers since high force output and high amplitude are mutually exclusive due to limited output work density of the actuators. The output work density (the work generated by the bending actuators divided by their volume) is $\bar{W} \sim \left(\frac{1}{2}\right)E\epsilon^2$ where E is the Young's modulus and ϵ is the strain.^[36] Due to deterministic nature of the work of adhesion, LCN output work density and the adhesive patch size are indeed only design parameters of interest in this work.

The mechanical properties of free-standing LCN cantilevers with different compositions were determined by dynamic mechanical analysis (DMA). Results showed that the Young's modulus of the LCN at room temperature increases from

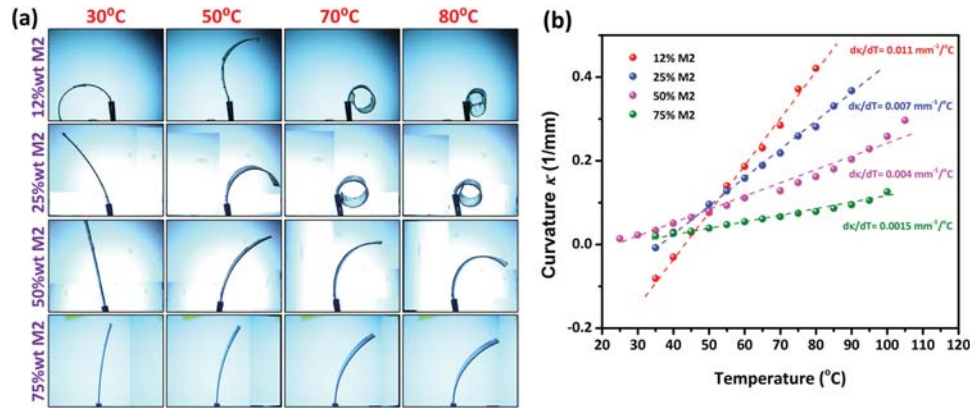


Figure 2. a) Side-view images of hybrid LCN cantilevers with different content of cross-linking mesogen subjected to thermal deformation (photos are taken during the cooling); b) variation of curvature with temperature.

30 MPa to 1.5 GPa when the M2 content increases from 12 to 75 wt%. Side-view images of thermal deformation of LCN cantilevers fixed at one end with different M2 contents are shown in **Figure 2a**. The curvature ($\kappa = 1/r$), where r is the radius of curvature, was measured by fitting the bent LCN to circular profile using ImageJ software. The temperature dependences of the curvature measured during cooling with different cross-linking contents are plotted in **Figure 2b**. The magnitude of thermal deformation ($\partial\kappa/\partial T$) decreases with increasing M2 content.

In order to calculate the output work density of the LCN cantilevers, both free tip displacement and blocked force (the maximum force generated at the free tip of LCN cantilever when it is fixed) need to be known. Therefore, two separate sets of experiments, similar to methods developed in,^[37,38] were performed to measure the blocked force and free tip displacement. In an arrangement shown in **Figure S3a** (Supporting Information) the free tip of the LCN beam was fixed by a stainless steel cantilever to block the thermal deformation. The maximum force at the LCN cantilever tip, F_{\max} , was measured and recorded by a force transducer during heating. The free tip displacement, δ_{\max} , is defined by the LCN cantilever tip deflection during thermal deformation without any constraint and was measured visually at different temperatures using a CCD camera, as can be seen in **Figure S3b** (Supporting Information). Note that unidirectional tip deflection cannot be used due to extremely large deformation of the LCN cantilevers. Instead, the arc length on the trajectory of thermally induced tip deflection that was projected on a virtual circle approximated the free tip displacement. Details of free displacement measurement and calculation are explained in Section SI-1 (Supporting Information).

Samples with 12% and 25% M2 content did not show sensible blocked force in the arranged setup. Therefore, LCN samples with 50%wt M2 content were chosen for the rest of studies. As both F_{\max} and δ_{\max} are temperature-dependent, the F_{\max} vs δ_{\max} curves must be plotted for characterization of the system at corresponding temperatures. As shown in **Figure S3d** (Supporting Information) for $1.3 \text{ mm} \times 2 \text{ mm} \times 0.188 \text{ mm}$ size LCN cantilevers, in first approximation, both F_{\max} and δ_{\max} vary linearly with temperature.^[39,40] **Figure 3** shows variation of blocked force versus free displacement at different temperatures. The

area under F_{\max} versus δ_{\max} curves represent the maximum mechanical work output that LCN cantilever provides. The work density of the cantilevers at each temperature is shown at the inset of **Figure 3**. It shows that the slope of the temperature dependence of the energy density is increasing with temperature and the values are similar to the output work density obtained for materials with similar chemical structures.^[41]

The bending energy of the LCN strip of Young's modulus E , area A , and thickness h is related to the curvature κ as $W_b = \frac{E\kappa^2 h^3 l w}{24(1-\sigma^2)}$ where σ is the Poisson ratio, w is the width, and l is the length of the LCN strip. Accordingly, LCN cantilevers with higher Young's modulus can generate greater work for peeling off the adhesive patch during the releasing. However, deformation of the stiffer LCN cantilevers takes place at higher temperatures and requires more thermal energy input. This will adversely influence the efficiency of the gripper and limits its applicability in transport of objects at lower temperatures. It is worth noting that the theoretical output work density of

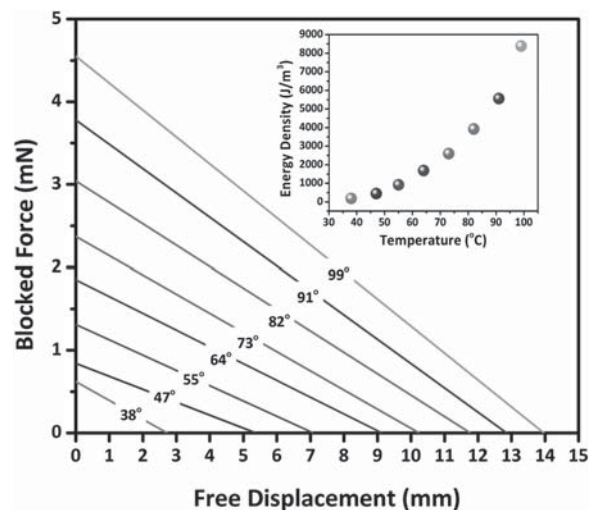


Figure 3. Blocked force versus free displacement for an LCN cantilever with $13 \times 2 \times 0.188 \text{ mm}^3$ size at different temperatures. The inset shows the variation of output energy density with temperature.

Table 1. Variation of theoretical and experimental output work density with temperature.

Temperature [°C]	Work density (experimental) [kJ m ⁻³]	Work density (theoretical) [kJ m ⁻³]
38	0.19	0.45
47	0.45	1.1
55	0.92	25
64	1.7	70.1
73	2.6	110
82	3.9	129
91	5.6	181
99	8.4	229

bending LCN actuators is usually obtained from room temperature modulus and the strain as $\bar{W} = \frac{1}{2} E \cdot \varepsilon^2$. Assuming a symmetric linear strain profile along the thickness, one can estimate the strain difference between top and bottom of the cantilever with respect to straight unbent position as $\varepsilon = \kappa h$. Using definition of energy in linear elasticity, theoretical energy density can be calculated by the measured Young's modulus, the curvature and the film thickness as $\bar{W} = \frac{1}{24} \frac{\kappa^2 h^2}{1 - \sigma^2} E$ and also can be estimated from the measured F_{\max} and δ_{\max} by $1/(lwh) \int_0^{\delta_{\max}} F_{\max} d\delta$. Those results are tabulated in **Table 1**. Results show that there is an increasing discrepancy between experimental and theoretical values of the output energy density at increasing temperatures. This is likely due to softening of the LCN cantilevers in higher temperature as seen in DMA results. That is, the softer they become the less output work they provide due to lower elastic modulus. Furthermore, the theoretical values are valid only for small deformations, which is not the case, especially at increasing temperatures. Systematic study on theoretical prediction of output energy density and elastic modulus will be the scope of our future work.

Physical properties of film-terminated fibrillar adhesives have been extensively investigated in other works^[13,14,35,42,43] and details are given in section SI-2, Supporting Information. Previous studies showed that the adhesion enhances when the thickness of the elastic terminal layer decreases and the thickness of the viscoelastic topcoat increases.^[13,14,35,42,43] Based on our previous results, the optimum thickness of the elastic terminal layer and the viscoelastic topcoat were set at 10 and 50 μm , respectively.^[14]

Two other parameters required for proper design of the gripper are "pull-off" and "preload" stress. These parameters are calculated by dividing the pull-off and preload forces by their corresponding contact area. The results are tabulated in the Table S1 (Supporting Information). The adhesion energy of the fibrillar surface was measured by calculating the area between the loading-unloading curves in an indentation cycle. Then, the overall work of adhesion (G), as a deterministic factor in design, was measured from the slope of the adhesion energy against maximum contact area and found to be 0.49 and 1.49 J m^{-2} for E-FT and VE-FT adhesives, respectively. Details are shown in Figure S5 (Supporting Information).

The maximum magnetic stress that an electromagnet with a magnetic field of 1T provides the maximum preload stress of ≈ 7 kPa. This preload stress is corresponding to pull-off stress of ≈ 35 kPa for VE-FT and ≈ 16 kPa E-FT (Table S1, Supporting Information). To lift and transfer a 4" silicon wafer with mass of ≈ 9 g, the minimum required size for the VE-FT and E-FT adhesive patches will be ≈ 2.8 and ≈ 6.4 mm^2 , respectively. Practical imperfections such as misalignment and non-constant or inadequate preload stress necessitates use of larger adhesive patches to guarantee secure transfer of delicate objects. However, the maximum size of the adhesive patch is limited to the output bending work of LCN cantilevers so they are able to propagate the crack at the adhesive interface for efficient releasing. Knowing the LCN work output versus temperature and overall work of adhesion for the VE-FT and E-FT, the maximum size of the adhesive patch that can self-peel via the bending of LCN cantilevers can be calculated at different temperatures from $W_b = G \cdot A_{\max}$. The maximum size of the adhesive patches of E-FT and VE-FT that an LCN cantilever with $13 \times 2 \times 0.188$ mm^3 size can peel off from a smooth flat substrate at 100 °C were obtained 84 and 28 mm^2 , respectively.

It is worth noting that both the work of adhesion and the bending energy of LCN depend on the surface temperature. Higher surface temperature could heat up the LCN faster, causing the larger and faster bending of LCN, which could in turn increase self-peeling speed of LCN (see the Supporting Information for additional details). Hence, temperature/rate-dependent dynamic effects are involved in our system. The rate-dependent behavior of fibrillar adhesives is well studied in the literature.^[44–48] It has been found that the speed of crack propagation increases as the retraction rate (i.e., the peeling rate in our case) increases, giving higher strain energy release rate or adhesive force. Indentation tests (Figure S6, Supporting Information) showed that the adhesive pull-off force of our adhesives increased with the retraction speed. This rate-dependent dynamic adhesion force should be taken into account in design and compensated for easy detachment. A similar case has been reported by Song and Sitti, where mushroom shaped micropillars on a soft inflatable membrane were used as a soft gripper for transferring of 3D objects. Due to viscoelastic dissipations, increment of the retraction speed during the unloading of adhered objects resulted in higher adhesion force. To compensate for these additional forces, they used higher inflated length or curvature during releasing.^[49] Herein, in a similar strategy, larger curvature of LCN cantilevers caused by the higher surface temperature (Figure 2) can result in the larger peeling angle during the detachment of the LCN adhesive patch so as to reduce the practical adhesion force; this situation spontaneously compensates for the excessive adhesion forces arising from dynamic viscoelastic effect. Even though the complex dynamic effects involved in our system have yet to be elucidated in future work, they are not expected to change the estimated maximum size of the adhesive patches much. Indeed, our experiments showed that the LCN adhesive pads designed using the parameters obtained at a constant temperature and speed can effectively release adhesion by the surface temperature-induced self-peeling of LCN, even though the adhesion force would be greater at higher temperature.

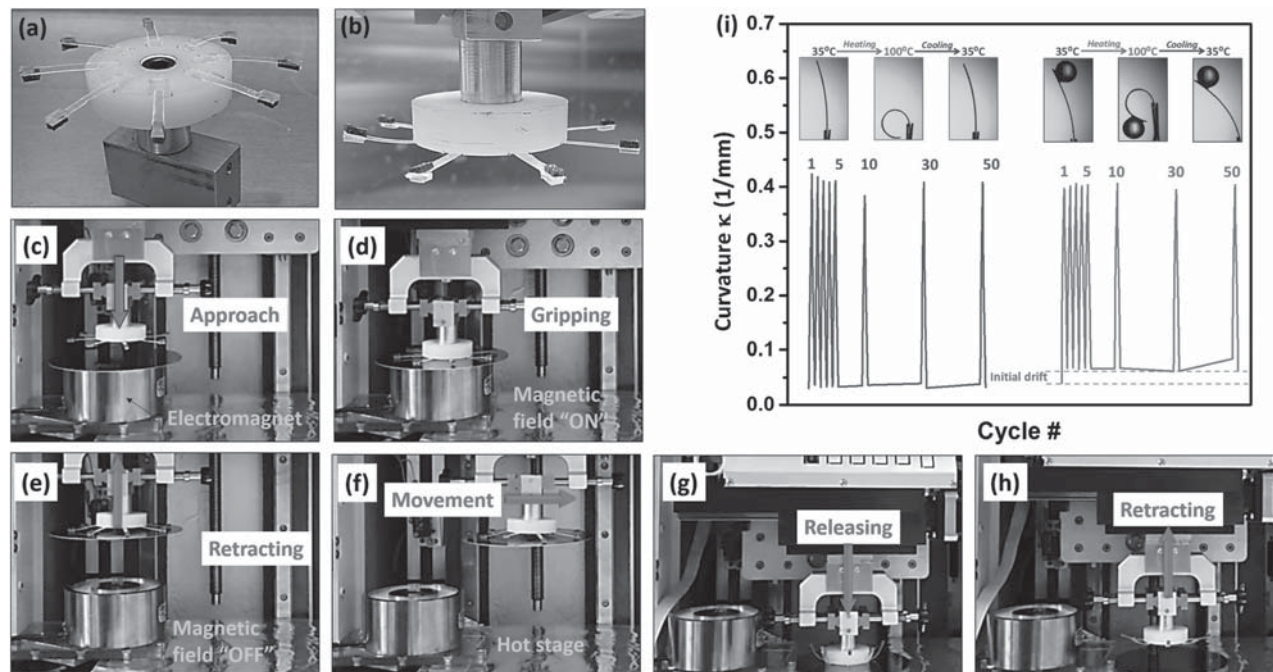


Figure 4. a, b) A multilegged gripper for pick-a-place automation, when it approaches toward the silicon wafer on c) an electromagnet stage. d) Normal gripping is facilitated by the magnetic field, and e) the silicon wafer is lifted when the electromagnet is in “off” state. f) Later movement is followed up by approaching the silicon wafer toward the hot stage and f) thermal bending deformation facilitates release; h) finally the gripper retracts back; i) variation of curvature with temperature after 50 cycles of heating and cooling for free and loaded cantilevers.

A prototype multilegged gripper was made as shown in Figure 4a,b. Misalignment with objects' center of gravity and undesired torque can be prevented by use of at least three legs. Our design is composed of eight LCN cantilevers, which are fixed at one end to an aluminum holder cylinder and attached to biomimetic fibrillar adhesive patches on the other end. The sizes of the adhesive patches were between minimum and maximum values calculated in the previous section (8–10 mm² for each cantilever). Magnetic patches of identical size are glued on the top of the adhesive patches to facilitate preloading by attractive magnetic stress. According to Figure 4c–h and Movies S1 and S2 (Supporting Information), gripping takes place by simple magnetic preloading and actuation of the LCN cantilevers toward the surface of the Si wafer using an electromagnet. Upon gripping, the electromagnet is turned off and the gripper cylinder is pulled upward to lift the object. After certain length of lateral movement, the gripper approaches toward the surface of a hot stage. Finally, in a mechanism similar to gecko toes back-scrolling, the releasing is rendered by self-peeling of the adhesive patches due to the bending deformation of hybrid LCN cantilevers. Movie S3 and Movie S4 show the side-view and bottom-view of a single cantilever and adhesive patch in contact with a transparent heating stage during the delamination. These movies confirm that the delamination of the adhesive patch is in the peeling mode and the peeling front develops from the cantilever tip toward the center of the gripper. By contrast, experiments were performed with non-patterned adhesive patches, showing very low gripping ability of the elastic non-patterned adhesives and very difficult releasing of the non-patterned adhesives with viscoelastic topcoats. As reported in the literature and our previous work, gecko-like patterned

adhesive patches have remarkably higher adhesion coefficients ($\mu' = F_{\text{pull-off}}/F_{\text{preload}}$) than their non-patterned counterparts, meaning that lower preloads are required to achieve higher adhesion pull-off forces, which is particularly beneficial for the gripping. On the other hand, surface microstructures alleviate the debonding instabilities of the viscous topcoats to avoid the cohesive failure of the adhesive during detachment.^[14,47]

The performance of such assembly and its applicability in industrial manipulation systems crucially depend on durability of both adhesive structures and LCN cantilevers.

Plastic distortion of the LCN cantilevers during repeating cycles of heating and cooling is identified as one of the potential factors affecting the maximum deformation amplitude and durability. Bending deformation at two loading regimes of 1) peeling off from the substrate and 2) after peeling might cause plastic distortions. During the peeling, the load on the cantilever can be approximated by the pull-off force of the adhesive patch to be ≈ 12.5 mN for the VE-FT. After peeling, the load on LCN can be approximated by weight of the adhesive and magnetic patches to be ≈ 0.7 mN. Thermal deformations of both free and loaded LCN cantilevers were examined in tests with multiple cycles, and results are shown in Figure 4i and Movies S5 and S6 (Supporting Information). We used a glass bead with weight of 0.7 mN to simulate the loaded deformation after peeling. Apparently, the magnitude of thermal deformation for free LCN cantilevers remains constant even after 50 cycles as shown in Figure 4 (left-side). For LCN cantilever loaded with ≈ 0.7 mN, there is a small drift in the second cycle. Thereafter, the magnitude of thermal deformation remains almost constant even after 50 cycles as shown in Figure 4 (right-side). Similarly, thermal cycling of the loaded cantilevers with ≈ 12.5 mN in very

low deformation range showed repeatable peeling behavior and only a slight plastic distortion.

To examine the reusability of gripper, the multiple adhesion measurements on a single spot of adhesive pads (E-FT and VE-FT) samples were first performed. As shown in Figure S7 (Supporting Information), the adhesion force of the E-FT sample remained the same up to 30 repeats. Whilst, the adhesion force for the VE-FT started to decay from the beginning and reached the 70% of its original value after 30 times repetition. Multiple gripping/releasing of a silicon wafer was also performed; they successfully repeated over 20 times with a gripper equipped with E-FT and VE-FT adhesive patches. Afterward, the gripper with the viscoelastic topcoat (VE-FT) started to lose performance, most likely, due to the plastic deformation of the topcoat and absorbing surface contamination. Thus, potential use of fully elastic fibrillar adhesives but with better adhesion performance, e.g., mushroom shaped fibrils, can help to ensure even better reusability.

Our results also show remarkable load bearing capability of the tested LCNs, which is equivalent to carrying loads up to 100 times of their own weight (0.125 mN), within their range of deformation. The outstanding deformability (i.e., displacement/length) of LCNs shown in this report and elsewhere,^[50] places them next to phase transition activated nanolayer bimorphs of Si/VO₂,^[36] polymer-CNT composite actuators and superior to the shape memory alloys, thermal expansion, and piezoelectric actuators.^[51] Thus, the Gecko-inspired self-peeling releasing mechanism shown in this work can be implemented in the development of novel micromanipulation systems without requiring sophisticated feedback control systems. Although only one type of thermoresponsive polyacrylate LCN system was tested here, variation of the molecular structure of the LCN cantilevers can create a great range of output energy densities up to 3000 kJ m⁻³.^[41] The attainable adhesion forces can be modulated by altering physical and geometrical properties of the adhesive pads.

To summarize, in this work the back-scrolling and self-peeling mechanism of gecko locomotion was mimicked using an LCN cantilever topped with a film-terminated fibrillar adhesive so as to make an effective gecko gripper. Output energy density of the LCN cantilevers along with their level of deformation was investigated by varying the level of network cross-linking. It is shown that LCN with moderate level of cross-linking provides sufficient output work to detach film-terminated adhesive patches from flat and smooth surfaces. The size of the adhesive patch is estimated from the LCN output work and work of adhesion. Self-peeling mechanism of the proposed structures was employed in pick and place handling of flat and smooth 2D objects. Results in this work can be deemed as a proof of concept for implementation of gecko-inspired back-scrolling mechanism for the development of switchable adhesives as soft grippers. Further, combination of high energy density and large deformation suggests that LCNs are good candidates for effective load bearing and large actuation. Future works will be focused on theoretical studies on the self-peeling mechanism of dry fibrillar adhesives backed with active materials and optimization of deformable materials mechanical performance using different groups of active materials.

Supporting Information

Supporting Information is available from the Wiley Online Library or from the author.

Acknowledgements

This work was supported by NSERC RGPIN-2014-04663 and an Early Researcher Award (ERA) from the Ontario Ministry of Research and Innovation and NSF DMR 1307674. The authors thank Julia Maier for photography, and Dr. N. M. Abukhdeir and Dr. A. Najafi Sohi for constructive discussions.

Received: July 28, 2016

Revised: September 25, 2016

Published online:

- [1] K. Autumn, Y. A. Liang, S. T. Hsieh, W. Zesch, W. P. Chan, T. W. Kenny, R. Fearing, R. J. Full, *Nature* **2000**, *405*, 681.
- [2] K. Autumn, A. Dittmore, D. Santos, M. Spenko, M. Cutkosky, *J. Exp. Biol.* **2006**, *209*, 3569.
- [3] N. Pesika, Y. Tian, B. Zhao, K. Rosenberg, H. Zeng, P. McGuiggan, K. Autumn, J. Israelachvili, *J. Adhes.* **2007**, *83*, 383.
- [4] K. Autumn, A. M. Peattie, *Integr. Comp. Biol.* **2002**, *42*, 1081.
- [5] K. Autumn, S. T. Hsieh, D. M. Dudek, J. Chen, C. Chitaphan, R. J. Full, *J. Exp. Biol.* **2006**, *209*, 260.
- [6] Y. Tian, N. Pesika, H. Zeng, K. Rosenberg, B. Zhao, P. McGuiggan, K. Autumn, J. Israelachvili, *Proc. Natl. Acad. Sci. USA* **2006**, *103*, 19320.
- [7] S. Hu, S. Lopez, P. H. Niewiarowski, Z. Xia, *J. R. Soc. Interface* **2012**, *9*, 2781.
- [8] A. K. Geim, S. V. Dubonos, I. V. Grigorieva, K. S. Novoselov, A. A. Zhukov, S. Y. Shapoval, *Nat. Mater.* **2003**, *2*, 461.
- [9] A. del Campo, E. Arzt, *Chem. Rev.* **2008**, *108*, 911.
- [10] M. P. Murphy, B. Aksak, M. Sitti, *Small* **2009**, *5*, 170.
- [11] D. Sameoto, C. Menon, *Smart Mater. Struct.* **2010**, *19*, 103001.
- [12] A. del Campo, C. Greiner, E. Arzt, *Langmuir* **2007**, *23*, 10235.
- [13] W. L. Noderer, L. Shen, S. Vajpayee, N. J. Glassmaker, A. Jagota, C.-Y. Hui, *Proc. R. Soc. A* **2007**, *463*, 2631.
- [14] H. Shahsavani, B. Zhao, *Macromolecules* **2014**, *47*, 353.
- [15] M. P. Murphy, S. Kim, M. Sitti, *ACS Appl. Mater. Interfaces* **2009**, *1*, 849.
- [16] S. Reddy, E. Arzt, A. del Campo, *Adv. Mater.* **2007**, *19*, 3833.
- [17] J. Cui, D.-M. Drotlef, I. Larraza, J. P. Fernández-Blázquez, L. F. Boesel, C. Ohm, M. Mezger, R. Zentel, A. del Campo, *Adv. Mater.* **2012**, *24*, 4601.
- [18] D. Liu, C. W. M. Bastiaansen, J. M. J. den Toonder, D. J. Broer, *Angew. Chem. Int. Ed. Engl.* **2012**, *51*, 892.
- [19] D. M. Drotlef, P. Blümmler, A. Del Campo, *Adv. Mater.* **2014**, *26*, 775.
- [20] M. Zhou, Y. Tian, D. Sameoto, X. Zhang, Y. Meng, S. Wen, *ACS Appl. Mater. Interfaces* **2013**, *5*, 10137.
- [21] J. Purtov, M. Frensemeier, E. Kroner, *ACS Appl. Mater. Interfaces* **2015**, *7*, 24127.
- [22] S. Kim, J. Wu, A. Carlson, S. H. Jin, A. Kovalsky, P. Glass, Z. Liu, N. Ahmed, S. L. Elgan, W. Chen, P. M. Ferreira, M. Sitti, Y. Huang, J. A. Rogers, *Proc. Natl. Acad. Sci. U S A* **2010**, *107*, 17095.
- [23] S. Kim, M. Spenko, S. Trujillo, B. Heyneman, V. Mattoli, M. R. Cutkosky, *Proc.- IEEE Int. Conf. Robot. Autom.* **2007**, 1268.
- [24] Q. Xu, Y. Wan, T. S. Hu, T. X. Liu, D. Tao, P. H. Niewiarowski, Y. Tian, Y. Liu, L. Dai, Y. Yang, Z. Xia, *Nat. Commun.* **2015**, *6*, 8949.
- [25] E. M. Terentjev, *J. Phys. Condens. Matter* **1999**, *11*, R239.

- [26] L. T. De Haan, V. Gimenez-Pinto, A. Konya, T. S. Nguyen, J. M. N. Verjans, C. Sánchez-Somolinos, J. V. Selinger, R. L. B. Selinger, D. J. Broer, A. P. H. J. Schenning, *Adv. Funct. Mater.* **2014**, *24*, 1251.
- [27] T. H. Ware, M. E. McConney, J. J. Wie, V. P. Tondiglia, T. J. White, *Science* **2015**, *347*, 982.
- [28] A. Sánchez-Ferrer, T. Fischl, M. Stubenrauch, A. Albrecht, H. Wurmus, M. Hoffmann, H. Finkelmann, *Adv. Mater.* **2011**, *23*, 4526.
- [29] A. L. Elias, K. D. Harris, C. W. M. Bastiaansen, D. J. Broer, M. J. Brett, *J. Mater. Chem.* **2006**, *16*, 2903.
- [30] D. Liu, D. J. Broer, *Angew. Chemie* **2014**, *126*, 4630.
- [31] R. R. Kohlmeier, J. Chen, *Angew. Chem. Int. Ed.* **2013**, *52*, 9234.
- [32] D. Liu, D. J. Broer, *Soft Matter* **2014**, *10*, 7952.
- [33] Z. L. Wu, A. Buguin, H. Yang, J.-M. Taulemesse, N. Le Moigne, A. Bergeret, X. Wang, P. Keller, *Adv. Funct. Mater.* **2013**, *23*, 3070.
- [34] H. Shahsavan, S. M. Salili, A. Jákli, B. Zhao, *Adv. Mater.* **2015**, *27*, 6828.
- [35] H. Shahsavan, B. Zhao, *Soft Matter* **2012**, *8*, 8281.
- [36] K. Liu, C. Cheng, Z. Cheng, K. Wang, R. Ramesh, J. Wu, *Nano Lett.* **2012**, *12*, 6302.
- [37] G. Yun, H. S. Kim, J. Kim, *Smart Mater. Struct.* **2008**, *17*, 025021.
- [38] J. Kim, Y. Kang, S. Yun, *Sens. Actuators, A Phys.* **2007**, *133*, 401.
- [39] E. Clarke, D. Kroening, F. Lerda, *Tools Algorithms Constr. Anal. Syst.* **2004**, *2988*, 168.
- [40] R. J. Wood, E. Steltz, R. S. Fearing, *Sens. Actuators A Phys.* **2005**, *119*, 476.
- [41] C. L. van Oosten, *PhD Thesis: Responsive Liquid Crystal Networks, Eindhoven University of Technology*, **2009**.
- [42] J. Liu, C. Y. Hui, A. Jagota, *J. Polym. Sci. Part B Polym. Phys.* **2009**, *47*, 2368.
- [43] J. Liu, C.-Y. Hui, L. Shen, A. Jagota, *J. R. Soc. Interface* **2008**, *5*, 1087.
- [44] X. Feng, M. A. Meitl, A. M. Bowen, Y. Huang, R. G. Nuzzo, J. A. Rogers, *Langmuir* **2007**, *23*, 12555.
- [45] S. Vajpayee, R. Long, L. Shen, A. Jagota, C.-Y. Hui, *Langmuir* **2009**, *25*, 2765.
- [46] U. Abusomwan, M. Sitti, *App. Phys. Lett.* **2012**, *101*, 211907.
- [47] W.-G. Bae, D. Kim, K.-Y. Suh, *Nanoscale* **2013**, *5*, 11876.
- [48] D. Labonte, W. Federle, *Soft Matter* **2015**, *11*, 8661.
- [49] S. Song, M. Sitti, *Adv. Mater.* **2014**, *26*, 4901.
- [50] T. J. White, D. J. Broer, *Nat. Mater.* **2015**, *14*, 1087.
- [51] T. Mirfakhrai, J. D. W. Madden, R. H. Baughman, *Mater. Today* **2007**, *10*, 30.